Available online at www.sciencedirect.com
ScienceDirect
Trans. Nonferrous Met. Soc. China 31(2021) 193−206
Transactions of Nonferrous Metals Society of China
www.tnmsc.cn

Improving hot corrosion resistance of aluminized TiAl alloy by anodization and pre-oxidation

Yuan-tao HU[1,2], Lei ZHENG[3], Hao-jie YAN[1,2], Lian-kui WU[1,2], Xiang-jun LIN[3], Fa-he CAO[1], Mei-yan JIANG[2]

1. School of Materials Science and Engineering, Sun Yat-sen University, Guangzhou 510275, China;
2. College of Materials Science and Engineering, Zhejiang University of Technology, Hangzhou 310014, China;
3. Institute of Defense Engineering, AMS, PLA, Beijing 100850, China

Received 3 March 2020; accepted 12 October 2020

Abstract: To shield TiAl alloy from hot corrosion attack, a compact protective coating was fabricated by the combination of aluminizing, anodization and pre-oxidation. The hot corrosion behavior of the coated-TiAl specimen was investigated in the mixture salt consisting of 75 wt.% Na_2SO_4 and 25 wt.% NaCl at 700 °C. Results indicated that the anodization and pre-oxidation were beneficial to the generation of Al_2O_3 layer, which could act as a diffusion barrier to prevent the molten salts and oxygen from diffusing into the alloy during exposure to a hot corrosion environment while the aluminizing coating could provide sufficient aluminum source to support the continuous formation of Al_2O_3 layer. Moreover, the internal stress of the coating was reduced due to the formation of a gradient coating consisting of $TiAl_3$ and $TiAl_2$.

Key words: hot corrosion; TiAl alloy; pack cementation; anodization; halogen effect

1 Introduction

Till now, much effort has been devoted to improving the mechanical properties and oxidation resistance of TiAl alloy, a promising substitute for nickel-based superalloy [1−6]. If used in aerospace, however, corrosive substances such as NaCl/KCl, Na_2SO_4/K_2SO_4 and Na_2VO_3 may deposit on TiAl alloys [7−11]. When service under elevated temperature, hot corrosion will occur between these salts and substrates, therefore destroying the protective surface oxides and accelerating the degradation of the alloys [12−17].

As well known, increasing aluminum content is an effective method to enhance the oxidation resistance of TiAl alloys [18]. This is because high Al content benefits the formation of an Al-enriched scale. But GODLEWSKA et al [9,19] reported that Ti−46Al−8Ta (at.%), Ti−46Al−8Nb (at.%) and Ti−6Al−1Mn (at.%) were all not resistant to corrosion when these alloys were contacted with salt deposits, e.g. Na_2SO_4 and/or NaCl at 700 and 800 °C. On the other hand, applying protective coating to prevent the contaminated salt from attacking the substrate is an efficient approach to improve the corrosion resistance of TiAl alloy [10,20−25]. TANG et al [20,21] investigated the influence of TiAlCr and enamel coatings on the hot corrosion resistance of TiAl alloys. Results showed that these two coatings exhibited good resistance against hot corrosion resistance for TiAl in $(Na,K)_2SO_4$ melts. Whereas, limited effect on the hot corrosion resistance was found when the TiAlCr coating was contaminated with Na_2SO_4 + NaCl melts. BACOS et al [26] found that chemical inertness Au-based coating could provide good corrosion resistance for Ti−48Al−2Cr−2Nb (at.%).

Corresponding author: Lian-kui WU; Tel: +86-20-39332297; E-mail: wulk5@mail.sysu.edu.cn
DOI: 10.1016/S1003-6326(20)65487-5

Additionally, Al−Y gradient coating, MCrAlY coating and NiCoCrAl−Y_2O_3 coating were also developed to improve the hot corrosion resistance for TiAl alloys [27−29].

Recently, we proposed to improve the oxidation resistance of Ti50Al alloy [30−33] and Ti45Al8.5Nb alloy [34] by anodization from NH_4F containing electrolyte. When exposed to air at elevated temperature, compact and adherent Al_2O_3 layer would be generated based on the halogen effect, therefore providing excellent oxidation resistance and spallation resistance. However, the dissolution effect of molten salt to Al_2O_3 makes the anodic film unstable and be consumed quickly under hot corrosion conditions [35,36]. Thus, anodization may only provide limited hot corrosion resistance for TiAl alloy in the initial stage.

To deal with this problem, an aluminizing coating was firstly prepared on TiAl alloy by pack cementation. Then, anodization in a fluorine-containing solution and pre-oxidation in air were conducted in sequence (Fig. 1). The aluminizing coating is expected to provide sufficient aluminum source for the formation of Al_2O_3, while anodization and pre-oxidation promote the generation of protective Al_2O_3 layer, therefore improving the hot corrosion resistance. The hot corrosion behavior was investigated in the mixture salt of 75 wt.% Na_2SO_4 + 25 wt.% NaCl at 700 °C. The protection mechanism of the aluminized and anodized TiAl alloy was also discussed.

2 Experimental

2.1 Materials and chemical reagents

As described in our previous studies [30−32], Ti−50Al (at.%) alloy, with the main phase consisting of γ-TiAl phase and a small amount of α_2-Ti_3Al was used as the substrate. The homogenized ingots were cut into 15 mm × 15 mm × 1.2 mm. All specimens were ground by emery paper with a grit of 60#, then cleaned ultrasonically in acetone and ethanol sequentially, and finally blow-dried with warm air.

2.2 Pack cementation of aluminizing coating

As described in our previous study [37], the aluminizing coating was prepared on TiAl alloys by pack cementation. Briefly, TiAl alloy was embedded by the pack mixtures with the composition of 10Al−5NH_4Cl−85Al_2O_3 (wt.%) in an alumina crucible. After being covered with alumina lid and sealed by silica sol binder, the crucible was put in a furnace chamber (cxzt−18−20, Shanghai Chenxin Electric Furnace Co., Ltd., China) with a vacuum about 2.0×10^{-2} Pa. The furnace was heated to 1000 °C at a rate of 5 °C/min, held at this temperature for 2 h, and then cooled to room

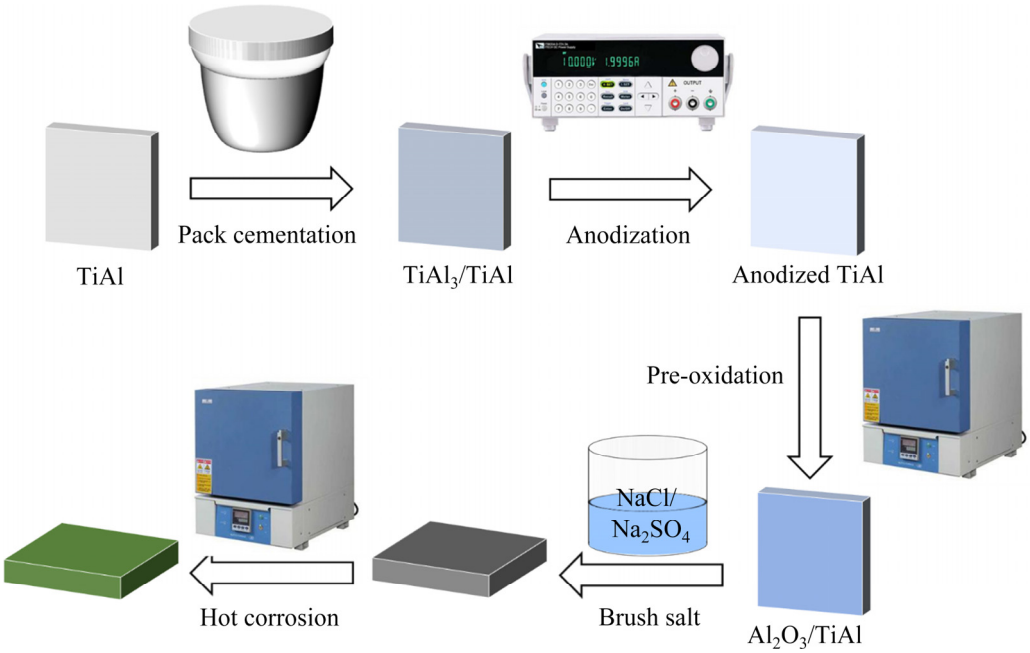

Fig. 1 Schedule illustration for pack cementation of aluminizing coating, anodization in NH_4F-containing electrolyte, pre-oxidation in air, salt deposition and hot corrosion test for TiAl alloy

temperature with finance. Finally, the samples were removed from the pack and ultrasonically cleaned to remove any loosely embedded pack materials.

2.3 Anodization

Anodization was performed as described in our previous study [34]. Briefly, two graphite plates (100 mm × 25 mm) were acted as the counter electrodes and placed face to face with a distance of ~5.0 cm. Aluminized TiAl alloy was hung in the middle of the two graphite plates, acting as the working electrode. Anodization was carried out in EG containing 0.15 mol/L NH_4F at 30 V for 1 h. After anodization, the specimens were taken out, cleaned and dried. The derived specimen was denoted as AA-TiAl alloy.

2.4 Pre-oxidation

Before hot corrosion test, the AA-TiAl alloy was pre-oxidized at 900 °C for 20 h in a muffle furnace (KSL−1200X, Hefei Kejing Materials Technology Co., Ltd, China). After pre-oxidation in air, the AA-TiAl alloy was denoted as POAA-TiAl alloy.

2.5 Hot corrosion test

The hot corrosion behavior of the POAA-TiAl alloy was investigated in another muffle furnace at 700 °C in static air. A eutectic salt mixture (75 wt.% Na_2SO_4 + 25 wt.% NaCl) with a melting point of 645 °C was employed for the hot corrosion test. Firstly, the oversaturated salt solution was prepared by dissolving the mixture salt into the deionized water. Then, a layer of salt film with the mass of (2.0±0.5) mg/cm^2 was deposited on the specimens by hand-brushing. During the hot corrosion process, the salt-coated specimen was put in the furnace with a temperature stabilized at 700 °C for 100 h. Three specimens were tested for each condition to ensure reproducibility.

After a certain interval of 20 h (the initial stage was only preserved for 5 h), the specimens were moved out from the furnace and cooled down to room temperature in air. Then they were washed in boiling deionized water for at least 10 min to dissolve and remove the salt and/or loose oxides on the surface. Thereafter, the specimens were taken out and dried off. The gross (with the exfoliated scale) and net (without the exfoliated scale) masses of the specimens were recorded by an electronic balance (0.1 mg precision, Sartorius BS124S). Then specimens were re-coated with salt to begin the next corrosion cycle.

2.6 Coating and corrosion scale characterization

The microstructure and composition of the specimens were characterized by scanning electron microscope (SEM, Carl Zeiss, Supra 55). X-ray diffraction (XRD) patterns of the specimens before and after oxidation were recorded on a Panalytical X'Pert PRO equipped with Cu K_α radiation (λ=0.154056 nm) at 40 kV and 40 mA.

3 Results

3.1 Morphology and composition of AA-TiAl alloy

As shown in Figs. 2(a) and (b), the AA-TiAl alloy is covered by a great deal of irregular particles that are composed of aluminum oxide according to the EDS analysis (Point 1 in Fig. 2(b) and Table 1). Whereas, no visible oxide particle is found in some regions (the inset in Fig. 2(b)). Interestingly, extremely high F content (10.25 at.%) is found in this region where the composition of Al to Ti is approximate to 3:1. EDS analysis (Point 3 in Fig. 2(c) and Table 1) and XRD pattern (Fig. 2(d)) indicate that the aluminizing coating with a thickness of ~15 μm still consists of $TiAl_3$ [38,39]. Additionally, Al_2O_3 with low diffraction intensity is also detected on the AA-TiAl alloy (the bottom part in Fig. 2(d)).

3.2 Morphology and composition of POAA-TiAl alloy

Figures 3(a) and (b) show the top-surface SEM images of the POAA-TiAl alloy. It is shown that pre-oxidation in air promotes the generation of a compact layer. Moreover, some follow-like Al_2O_3 particles are found on the specimen surface (inset in Fig. 3(b) and Point 1 in Table 2). While other region is Al_2O_3 enriched (Points 2 and 3 in Fig. 3(b) and Table 2). Cross-sectional SEM image and corresponding EDS analysis results reveal that an obvious $TiAl_2$ layer can be found between the aluminized $TiAl_3$ layer and the TiAl substrate (Fig. 3(c)). XRD pattern confirms that besides $TiAl_3$ and Al_2O_3, $TiAl_2$ is also detected in the POAA-TiAl alloy (Fig. 3(d)).

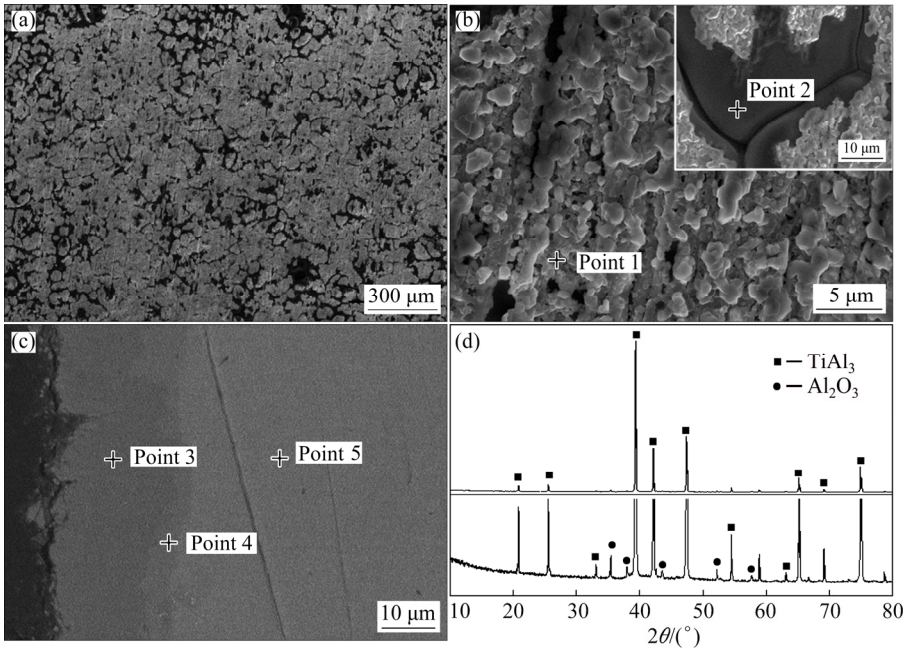

Fig. 2 Top surface (a, b) and cross-sectional (c) SEM images and XRD pattern (d) of AA-TiAl alloy (The inset in (b) is enlarged from the flat region; the curve at the bottom part in (d) is the enlarged pattern)

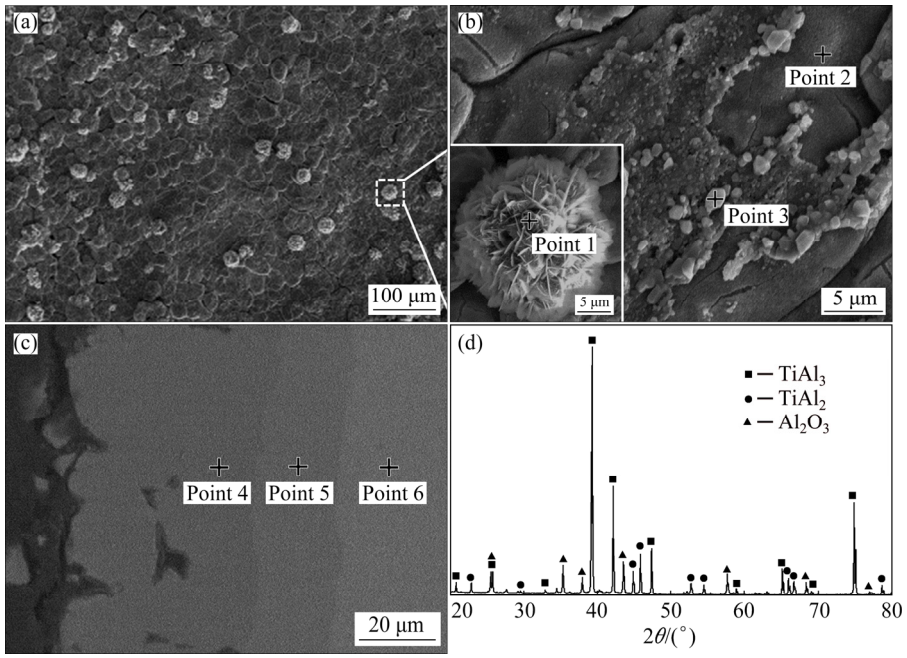

Fig. 3 Top surface (a, b) and cross-sectional (c) SEM images and XRD pattern (d) of POAA-TiAl alloy (The inset in (b) is enlarged from one particle marked in (a))

Table 1 EDS results of regions marked in Fig. 2 (at.%)

Point	Ti	Al	O	F
1	0.20	31.25	68.55	−
2	18.15	59.29	12.32	10.25
3	23.80	71.87	4.33	−
4	34.67	62.18	3.15	
5	47.43	50.25	2.32	−

Table 2 EDS results of regions marked in Fig. 3 (at.%)

Point	Ti	Al	O
1	–	47.61	52.39
2	1.21	31.86	66.93
3	6.69	31.97	61.34
4	24.00	70.02	5.98
5	31.39	63.59	5.02
6	47.93	48.78	3.29

3.3 Hot corrosion kinetics curves and optical images

The hot corrosion kinetics curves of the POAA-TiAl alloy with a mixture salt deposit of 75 wt.% Na_2SO_4 + 25 wt.% NaCl at 700 °C are shown in Fig. 4. Both the gross (with the exfoliated scale) and net mass gains (without the exfoliated scale) are presented. The data of the aluminized and AA-TiAl alloys are also given for comparison. As shown in Fig. 4(a), the total mass gain of the aluminized TiAl alloy after 100 h of hot corrosion was 12.34 mg/cm^2. While the total mass gains of the AA- and POAA-TiAl alloys dramatically reduce to 4.32 and 1.82 mg/cm^2, respectively, which are 35.01% and 14.75% that of the aluminized TiAl alloy.

The net mass gains of the specimens are shown in Fig. 4(b). For the aluminized TiAl alloy, after an increase in the initial stage up to 20 h, the mass reduces slightly, then alternately increases and decreases. While obvious different phenomena are observed on the AA- and POAA-TiAl alloys. Both of the net mass increase monotonously during the whole test.

After the hot corrosion test, the optical images of these specimens were also taken. As shown in Fig. 5(a), loose corrosion scale with poor adhesion to the substrate is observed on the aluminized TiAl alloy. Besides, obvious scale spallation is found. Whereas, only localized spallation and a handful of cracks are observed on the corrosion scale generated on AA-TiAl alloy (Fig. 5(b)). In the case of POAA-TiAl alloy (Fig. 5(c)), an intact corrosion

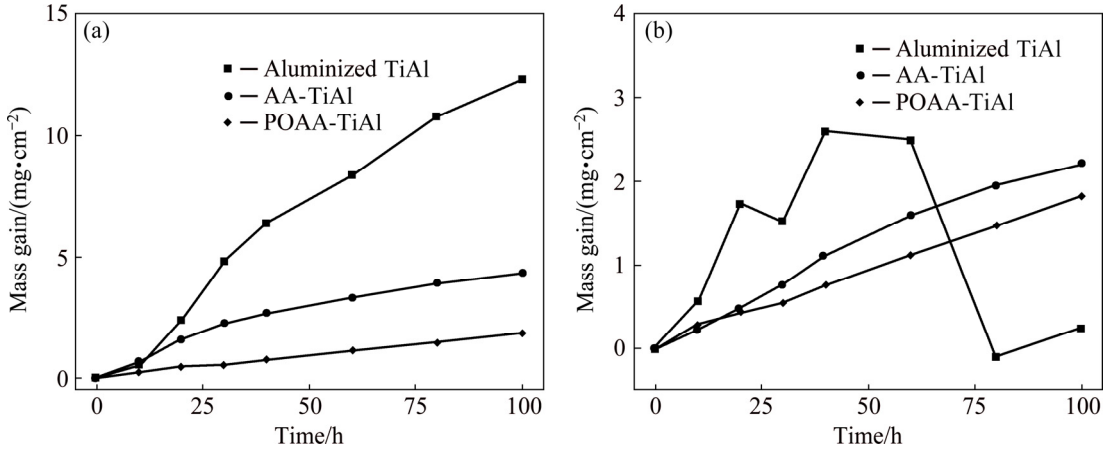

Fig. 4 Gross (with exfoliated scale) (a) and net (without exfoliated scale) (b) mass gains of aluminized, AA-, and POAA-TiAl alloys during hot corrosion at 700 °C

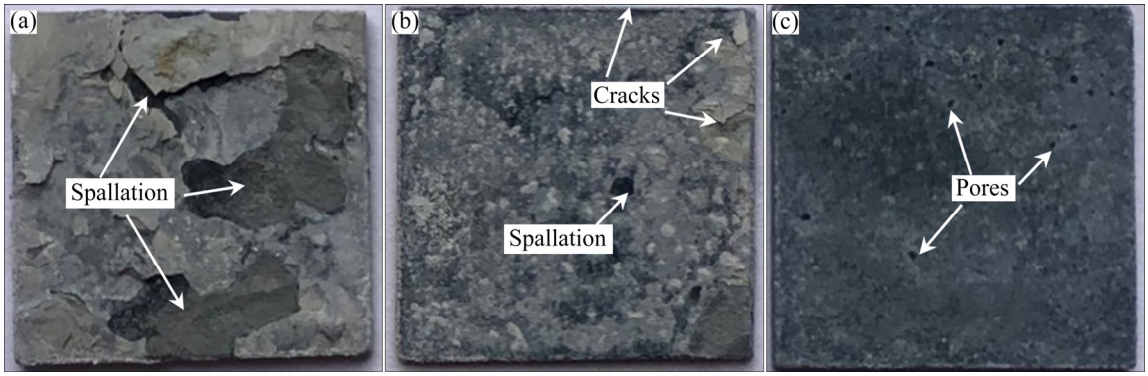

Fig. 5 Optical images showing macro-morphologies of aluminized (a), AA- (b), and POAA- (c) TiAl alloys after hot corrosion for 100 h

scale with some pores emerges and no spallation is found during the whole hot corrosion test.

3.4 Composition of corrosion scale

As shown in Fig. 6(a), after 100 h hot corrosion, the corrosion scale on aluminizing TiAl alloy is composed of TiO_2, Al_2O_3 and $Na_2Ti_6O_{13}$. Moreover, the diffraction peaks, i.e. $TiAl_3$ and $TiAl_2$ derived from the aluminizing coating are also detected. The exfoliated scale was collected and the composition was determined by XRD. As shown in Fig. 6(b), the diffraction peaks are ascribed to NaCl, Na_2SO_4, TiO_2 and Al_2O_3. NaCl and Na_2SO_4 are derived from the contaminated salt. A similar XRD pattern is observed on the AA-TiAl alloy, except for the difference in the diffraction intensity (Fig. 6(c)). In this case, Al_2O_3 becomes the dominant component, and the diffraction intensities of $TiAl_3$ and $TiAl_2$ are enhanced. For the POAA-TiAl alloy (Fig. 6(d)), although TiO_2, Al_2O_3, $TiAl_3$ and $TiAl_2$ are still detected, $TiAl_3$ and $TiAl_2$ turn to be the dominant components. Besides, $Na_2Ti_6O_{13}$ disappears and $Na_2Al_2Ti_6O_{16}$ newly emerges.

3.5 Morphology of corrosion scale

As shown in the low magnified SEM image (Fig. 7(a)), a rugged surface with various ravines and severe spallation is found on the aluminized TiAl alloy after 100 h hot corrosion. Additionally, there are lots of protrusions and cracks on the scale (Fig. 7(b)). Magnified SEM image and corresponding EDS analysis reveal that the cluster mainly consists of Al_2O_3 (Point 1 in Fig. 7(c) and Table 3), while the flake structure is composed of TiO_2 and $Na_2Ti_6O_{13}$ (Point 2 in Fig. 7(c) and Table 3). In the case of AA-TiAl alloy, there are two typical morphologies. As shown in Figs. 7(d) and (e), a relatively compact scale consisting of flake structure is found in some regions. Other region is composed of blocks that are separated by abundant cracks (Fig. 7(f)). EDS analysis indicates that although these two regions are composed of Al and Ti mixture oxides, higher Al is detected from the former region (Point 3 in Table 3). But much higher Na and Cl contents are found in the latter region (Point 4 in Table 3). For POAA-TiAl alloy, a relatively compact corrosion scale is observed

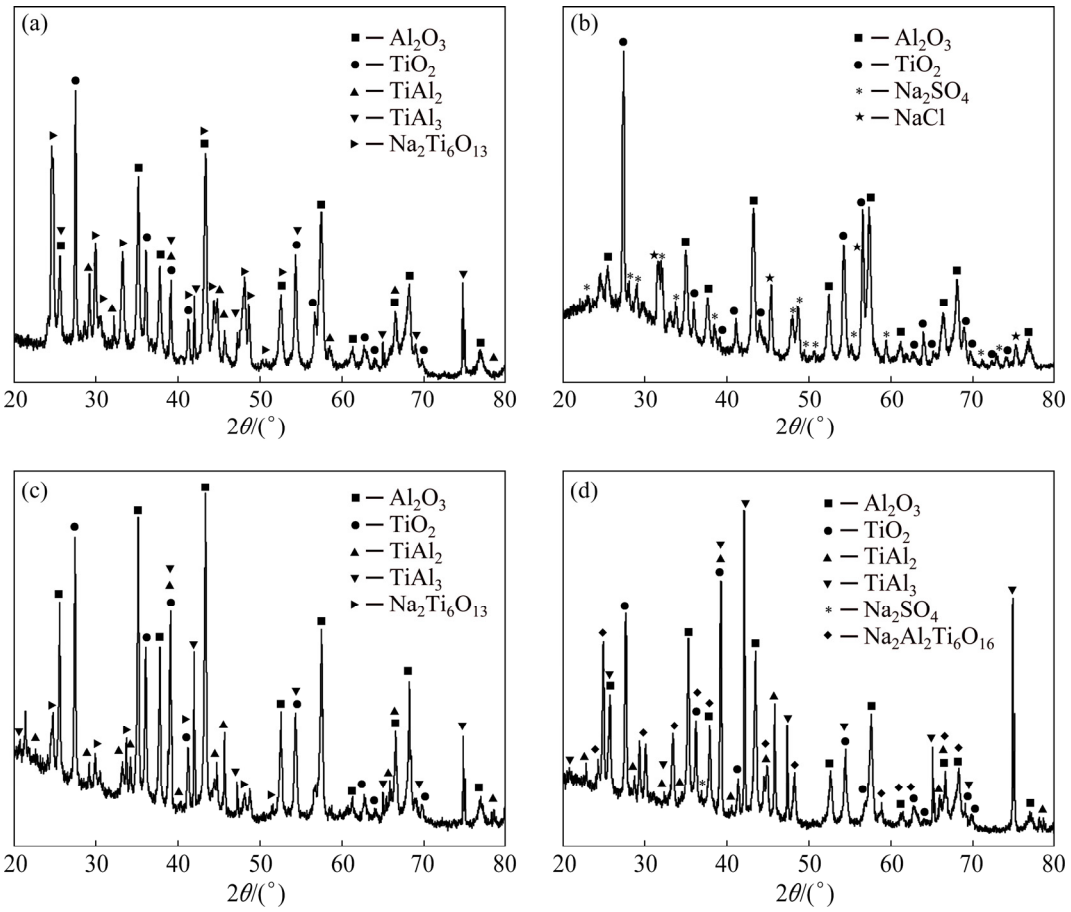

Fig. 6 XRD patterns of aluminized (a, b), AA- (c), and POAA- (d) TiAl alloys after hot corrosion at 700 °C for 100 h ((a) and (b) are derived from the specimen and exfoliated scale, respectively)

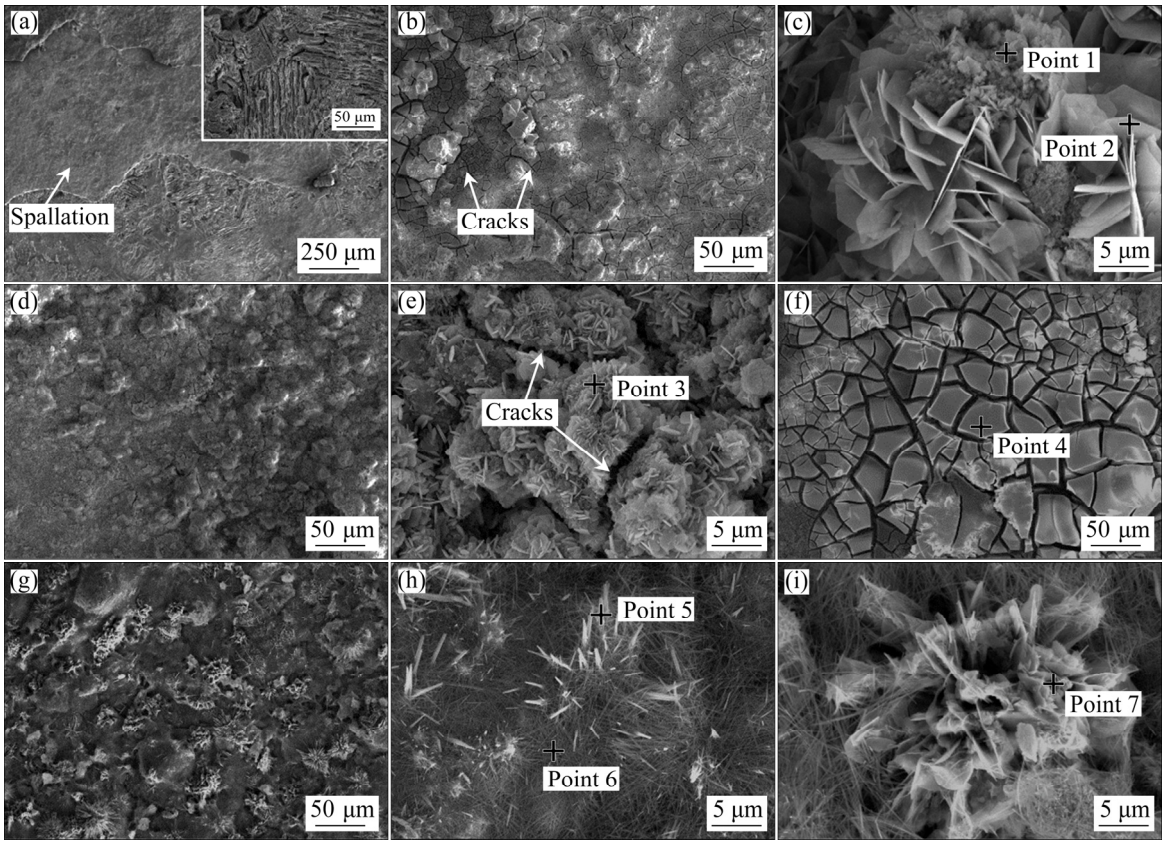

Fig. 7 Top-surface SEM images of aluminized (a−c), AA- (d−f), and POAA- (g−i) TiAl alloys after hot corrosion at 700 °C for 100 h (The symbols marked in each image show the regions where EDS analysis was carried out)

(Fig. 7(g)). Magnified SEM images and EDS analysis indicate that the needle-like structure is titanium enriched and composed of TiO_2 and $Na_2Al_2Ti_6O_{16}$ based on the XRD pattern (Points 5 and 6 in Fig. 7(h) and Table 3). The flower-like particle is aluminum enriched (Point 7 in Fig. 7(i) and Table 3).

Table 3 EDS results of regions marked in Fig. 7 (at.%)

Point No.	Ti	Al	O	Na	Cl	S
1	4.44	23.43	69.63	2.03	0.12	0.35
2	14.76	0.31	67.50	16.92	0.02	0.49
3	8.85	16.63	70.26	4.21	0.03	0.01
4	8.12	8.81	70.52	8.29	3.95	0.31
5	17.48	1.67	71.87	8.65	0.03	0.02
6	15.84	0.89	74.43	8.73	0.09	0.02
7	4.35	31.55	63.20	0.69	0.07	0.13

The cross-sectional SEM images and corresponding EDS analysis of the specimens underwent hot corrosion test are displayed in Figs. 8 and 9. One should be kept in mind that obvious scale spallation occurs on aluminized TiAl alloy. Thus, a simple comparison of the apparent thickness of the residual corrosion scale is meaningless. As shown in Fig. 8(a), a few through-thickness cracks, which are perpendicular to the substrate are found in the corrosion scale. The distribution of Al, Ti and O elements was analyzed by the EDS line scan from the outmost layer of the corrosion scale to the TiAl substrate. As shown in Fig. 8(c), Al, Ti, O and Na are detected from the outmost layer (Region I). Then an aluminum-enriched inner layer with a thickness of 15−30 μm is observed (Region II). Beneath this layer, there is an aluminum dominated layer but with lower aluminum content (Region III). EDS measurement demonstrates that the corrosion scale is composed of Al and Ti mixture oxides (Point 1 in Table 4). Besides, Na, Cl and S are also detected in this region. Notably, the component filled in the crack is Al_2O_3 dominant (Point 2 in Table 4) and the aluminizing coating still consists of $TiAl_3$ (Point 3 in Table 4).

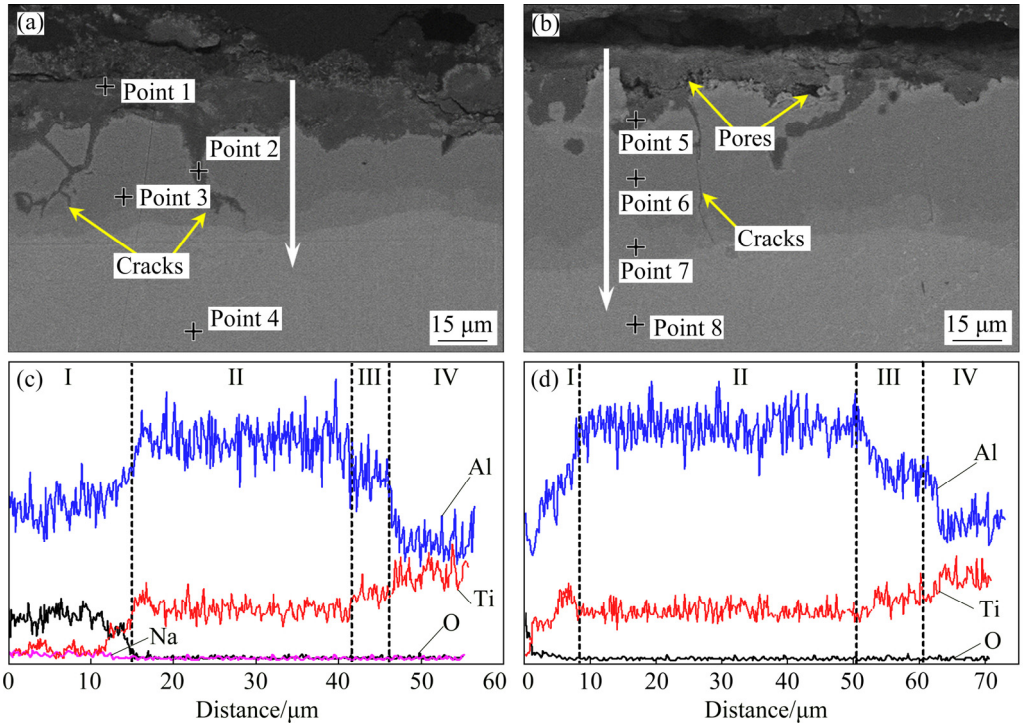

Fig. 8 Cross-section SEM images (a, b) and corresponding EDS element line scan results (c, d) of aluminized (a, c) and AA- (b, d) TiAl alloys after hot corrosion at 700 °C for 100 h (The arrows in (a) and (b) show the direction and position where the EDS line scan analysis was carried out; the spots marked in (a) and (b) represent the sites for EDS measurement)

For AA-TiAl alloy, some pores are observed in the corrosion scale (Fig. 8(b)). Although through-thickness cracks can still be found in the aluminizing coating, no obvious corrosion product is filled in it, indicating that the internal oxidation is suppressed. EDS analysis shows that the corrosion scale is Al-enriched (Point 5 in Fig. 8(b) and Table 4, Fig. 8(d)). Beneath this layer, there are two layers consisting of $TiAl_3$ (Point 6 in Fig. 8(b) and Table 4) and $TiAl_2$ (Point 7 in Fig. 8(b) and Table 4), respectively.

As shown in Fig. 9(a), the corrosion scale generated on POAA-TiAl alloy is well adherent to the substrate, and only a few pores are observed in the corrosion scale. EDS line scan results reveal that the composition of the corrosion scale is similar to that on the AA-TiAl alloy, except for the much thicker aluminizing coating (Fig. 9(b)). EDS analysis indicates that Ti content in the corrosion layer is extremely low (Fig. 9(c), Point 1 in Fig. 9(a) and Table 5) and the content increases from the corrosion layer to the aluminizing coating (Figs. 9(c−f), Points 1−4 in Fig. 9(a) and Table 5). While the Al content performs the opposite rule.

4 Discussion

When exposed to a molten salt environment, a loose and porous TiO_2 based layer will generate on TiAl alloy. Then, molten salt ions and oxygen can easily penetrate into the substrate through this non-protective layer and accelerate the corrosion process. Moreover, the dissolution of TiO_2 layer by molten salt further damages the corrosion scale [9]. Applying barrier coating on TiAl alloy against the inward diffusion of molten ions is an efficient strategy to enhance the hot corrosion resistance.

Aluminizing coating fabricated by pack cementation has been demonstrated as an effective method to improve the oxidation resistance of TiAl alloy [37,40], whereas the quick consumption of aluminum by molten salt may result in limited corrosion resistance. As shown in Fig. 5, severe spallation occurs on the aluminized TiAl alloy during the hot corrosion test. The top surface and cross-section morphologies indicate that many thicknesses-through-cracks are found in the corrosion scale (Figs. 7(a) and 8(a)).

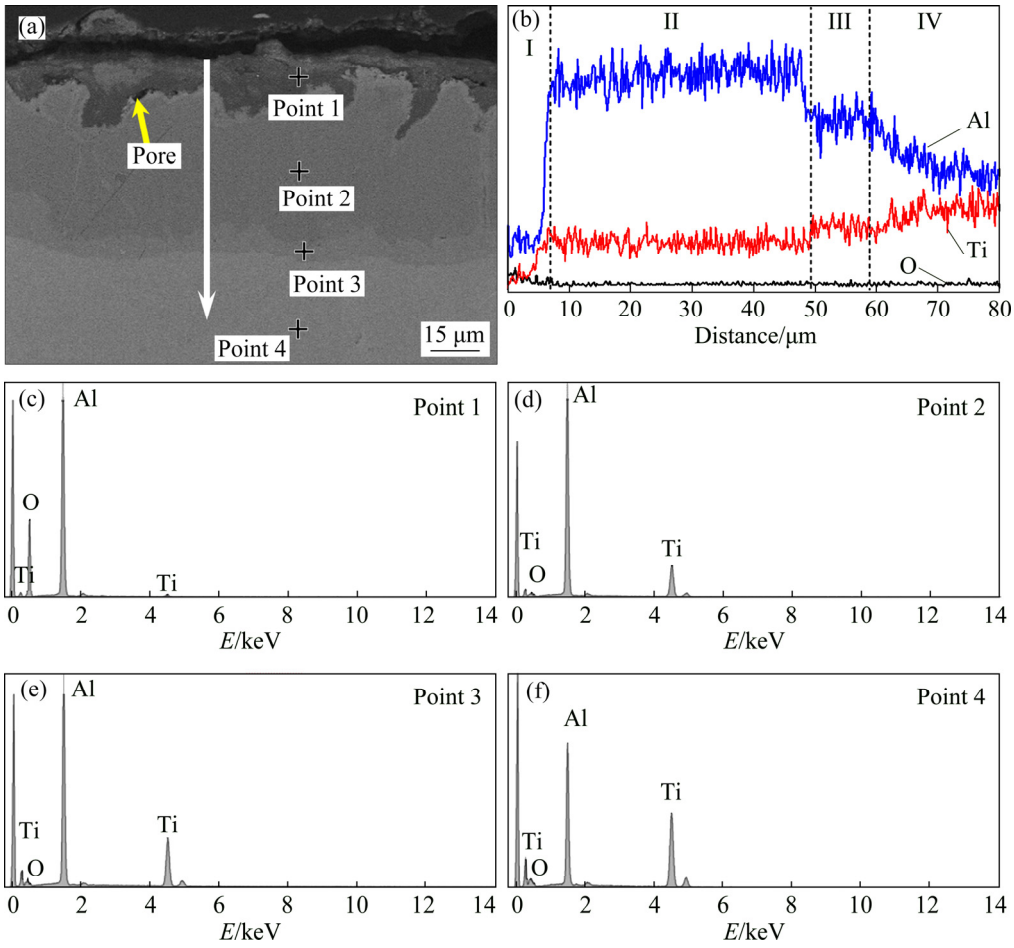

Fig. 9 Cross-section SEM image (a) and corresponding EDS element line scan results (b) of POAA-TiAl alloys after hot corrosion at 700 °C for 100 h, and EDS spectra (c−f) derived from Points 1−4 marked in (a) (The arrow in (a) shows the direction and position where the EDS line scan analysis was carried out; the spots marked in (a) represent the sites for EDS measurement)

Table 4 EDS results of regions marked in Fig. 8 (at.%)

Point No.	Ti	Al	O	Na	Cl	S
1	18.40	11.89	61.75	6.34	1.58	0.03
2	1.18	38.86	59.37	–	0.59	–
3	24.16	70.21	5.62	–	–	–
4	46.18	45.05	8.77	–	–	–
5	9.34	26.23	62.78	0.73	0.15	0.04
6	23.80	71.87	4.33	–	–	–
7	30.41	60.36	9.23	–	–	–
8	41.60	50.25	8.15	–	–	–

Table 5 EDS results of regions marked in Fig. 9 (at.%)

Point No.	Ti	Al	O	Na	Cl	S
1	1.38	37.73	60.61	0.25	0.02	0.01
2	23.12	71.71	5.17	–	–	–
3	30.39	61.59	8.02	–	–	–
4	44.75	41.93	13.32	–	–	–

During the initial hot corrosion process, the aluminizing coating will be selectively oxidized to form Al_2O_3, which can prevent molten salt ions and oxygen from diffusing into the substrate to some extent. As illustrated in Fig. 10(a), prolonging the exposure time results in the generation of non-protective Al_2O_3 and TiO_2 mixture oxides. Because the service temperature (700 °C) is higher than the melting point of the mixture salt (684 °C), the following reaction will occur at the molten salt/oxide layer interface [23,41]:

$$2Na_2SO_4 \rightarrow 2Na_2O+2S+3O_2 \quad (1)$$

With the proceed of hot corrosion, the activity of sulphur gradually increases and promotes the formation of sulfide at the scale/aluminizing coating. Meanwhile, the generated Na_2O will react

with Al_2O_3 based on alkaline dissolution:

$$Al_2O_3+O^{2-}\rightarrow 2AlO_2^- \quad (2)$$

The dissolution of AlO_2^- into molten salt leads to the formation of concentration gradient from the scale/substrate interface to the scale/air interface. With the gradually reduced alkalinity, the outward diffused AlO_2^- will decompose and deposit in the form of loose and unprotected Al_2O_3 particle as follows:

$$2AlO_2^-\rightarrow Al_2O_3+O^{2-} \quad (3)$$

The repeated process between Reactions 2 and 3 not only leads to the generation of loose and porous Al_2O_3 but also accelerates the consumption of Al.

Moreover, under high temperature the extremely aggressive NaCl will react with oxygen from air and TiO_2/Al_2O_3 mixture oxides as well as the substrate, according to the following reactions:

$$4NaCl+2Al_2O_3+O_2\rightarrow 4NaAlO_2+2Cl_2 \quad (4)$$

$$4NaCl+12TiO_2+O_2\rightarrow 2Na_2Ti_6O_{13}+2Cl_2 \quad (5)$$

$$2NaCl+2Al+2O_2\rightarrow 2NaAlO_2+Cl_2 \quad (6)$$

$$4NaCl+12Ti+13O_2\rightarrow 2Na_2Ti_6O_{13}+2Cl_2 \quad (7)$$

Two effects will be exhibited by chlorine released from the above reactions. For one thing, the generated chlorine gas can destroy the continuity of the oxide scale, leading to the formation of pores and cracks. For another, the penetrated chlorine can react with the aluminizing coating and form volatile chlorides, e.g. $TiCl_2$, $TiCl_4$ and $AlCl_3$:

$$Ti+Cl_2\rightarrow TiCl_2 \quad (8)$$

$$Ti+2Cl_2\rightarrow TiCl_4 \quad (9)$$

$$2Al+3Cl_2\rightarrow 2AlCl_3 \quad (10)$$

The accumulation of these chlorides with high saturated vapor pressure at the corrosion scale/aluminizing coating interface results in the generation of cracks. Moreover, the outward diffused chlorides will react with oxygen from air:

$$TiCl_2+O_2\rightarrow TiO_2+Cl_2 \quad (11)$$

$$TiCl_4+O_2\rightarrow TiO_2+2Cl_2 \quad (12)$$

$$4AlCl_3+3O_2\rightarrow 2Al_2O_3+6Cl_2 \quad (13)$$

The above self-sustaining reactions lead to the generation of a non-protective scale on the aluminized TiAl alloy.

As shown in Fig. 10(a), with the proceeding of hot corrosion the aluminizing coating will be rapidly consumed. Meanwhile, the inter-diffusion between the aluminizing coating and TiAl substrate, together with the inward diffusion of molten salt ions and oxygen cause the generation of pores and cracks in the coating. Then, the outward diffused Ti

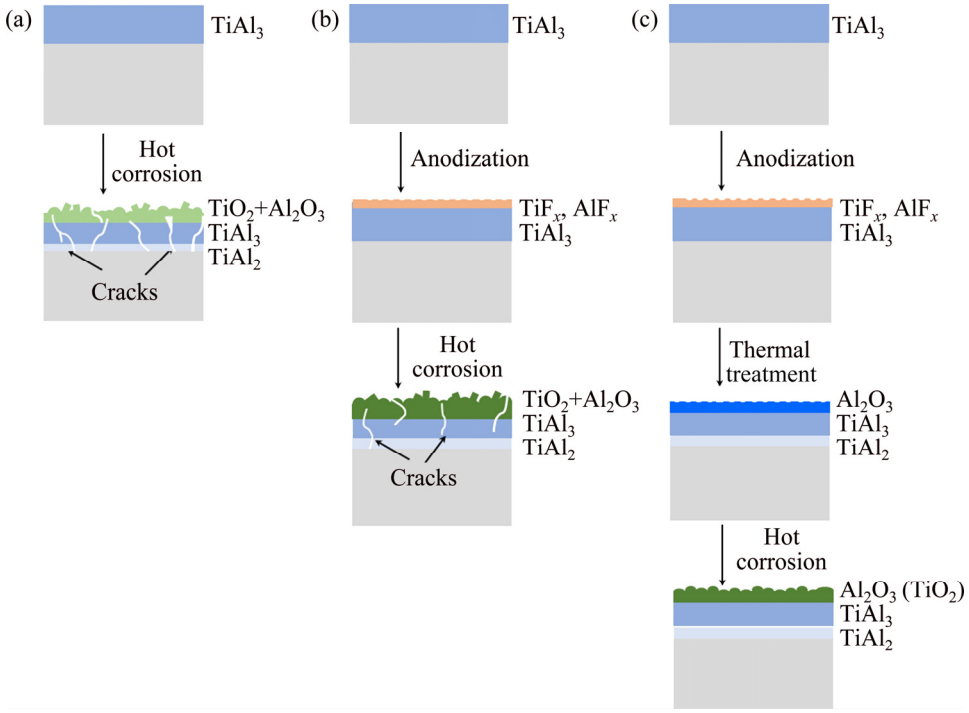

Fig. 10 Schematic illustration for hot corrosion process of aluminized (a), AA- (b), and POAA- (c) TiAl alloys in 75 wt.% Na_2SO_4 + 25 wt.% NaCl salt deposited at 700 °C

will reach the aluminizing coating/corrosion scale interface and be oxidized to porous and non-protective TiO_2. The rapid growth of TiO_2 results in great growth stress, and then promotes the scale to exfoliate from the substrate. Therefore, when contaminated with Na_2SO_4/NaCl mixture, the rapid consumption of aluminizing coating and spallation of the corrosion scale will lead to poor hot corrosion resistance.

As illustrated in Fig. 10(b), anodization in a fluorine-containing solution results in the generation of an aluminum and fluorine enriched anodic film (Fig. 2). During the hot corrosion test, the evolution of fluorine components, including TiF_x and AlF_x, will promote the formation of Al_2O_3 based on the halogen effect [31,42−44]. In detail, the evaporation of TiF_x with a low boiling point promotes the enrichment of Al in the aluminizing coating. Moreover, the reaction between oxygen from the air and outward diffused AlF_x from anodic film promotes the formation of Al_2O_3, which can fill in the pores and cracks in the anodic film. This Al_2O_3-enriched layer can not only prevent the inward diffused molten salt ions and oxygen but also impede the outward diffusion of Al and Ti. Therefore, the hot corrosion resistance of the TiAl alloy is improved (Fig. 4(a)). However, some pores and localized scale spallation are observed on the AA-TiAl alloy (Fig. 5(b)). And many cracks are also found in the corrosion scale (Fig. 7(f)). This is because the non-compact anodic film on the TiAl alloy provides pathways for diffusion species (Fig. 2). Moreover, only thin and non-continuous Al_2O_3 will be generated on the anodized TiAl alloy when directly exposed to hot salt environment. Aggressive molten salt ions can penetrate into the aluminizing coating and TiAl substrate, therefore destroying the AA-TiAl alloy.

While before exposure to the hot corrosion environment, pre-oxidation in air promotes the formation of a compact and adherent Al_2O_3 layer on aluminized TiAl alloy (Fig. 10(c)). Additionally, during the pre-oxidation process, the pores and cracks in the anodic film can be filled with oxides. Thus, a protective Al_2O_3-enriched layer is formed before the application of a mixture of salt deposits (Fig. 3). Besides, pre-oxidation results in the generation of gradient aluminizing coating consisting of $TiAl_3$ and $TiAl_2$, which benefits to reduce the internal stress and improve the crack and spallation resistance. Results demonstrate that the POAA-TiAl alloy provides good resistance against hot corrosion and no scale spallation is found. It should be noted that although Al_2O_3 will be generated both on AA-TiAl alloy and POAA-TiAl alloy, obvious difference emerges on them. For the former, owing to the halogen effect, thin and non-continuous Al_2O_3 will be generated during the initial hot corrosion process. In this case, the inward diffused molten salt ions and oxygen can also react with the aluminizing coating, leading to the generation of a mixed oxide scale. As for the latter, continuous and adherent Al_2O_3 layer will be generated during the pre-oxidation stage. This protective Al_2O_3 layer not only efficiently prevents the inward diffusion of molten salt ions and oxygen, but also dramatically slows down the consumption of the aluminizing coating. This has been confirmed from the morphologies, where no obvious difference is found in the aluminizing coating before and after the hot corrosion test. Thus, the hot corrosion resistance of the AA-TiAl alloy is further enhanced by pre-oxidation in air.

Similarly, XU et al [45] fabricated a gradient Al_2O_3/Al composite coating on Ti−46.5A1−4V−1.0Cr (wt.%) alloy by a two-step magnetron sputtering method [45]. As expected, the Al_2O_3 top layer could effectively suppress the erosion of Na^+, O^{2-} and S^{2-}, while the Al interlayer could provide sufficient Al source for the formation of Al_2O_3. Results showed that although the hot corrosion resistance of the composite coating with Na_2SO_4 deposit was improved at 850 °C, visible defects were found at the coating/substrate interface after 100 h of hot corrosion. This may be attributed to the poor adhesion property between the Al_2O_3 top layer and Al interlayer. However, in the present work, the Al_2O_3 layer was generated in-situ from the aluminizing coating. Moreover, the protective Al_2O_3 layer will be continuously produced due to the low oxygen partial pressure at the coating/alloy interface and the sufficient Al source from the aluminizing coating.

5 Conclusions

(1) Aluminizing coating only provided limited resistance against the hot corrosion with Na_2SO_4 +

NaCl mixture salt deposited at 700 °C. A loose corrosion scale was found on the substrate and severe spallation occurred during the test.

(2) Anodization in a fluorine-containing solution resulted in the generation of Al-enriched layer. Whereas the cracks in the anodic film could provide pathways to the inward diffused molten salt ions and oxygen. Thus, although the corrosion resistance of the aluminizing coating was improved by anodization, cracks and localized spallation were still observed on the corrosion scale.

(3) Pre-oxidation in air promoted the generation of a compact and protective Al_2O_3 layer, which could efficiently prevent the aggressive species from attacking the substrate and rapid consumption of the aluminizing coating. Moreover, the generation of gradient coating consisting of $TiAl_3$ and $TiAl_2$ benefits to reduce the coating internal stress. Therefore, the POAA-TiAl alloy provided excellent resistance against hot corrosion. No scale exfoliation was observed and the Al_2O_3 dominant outmost scale was generated after 100 h of corrosion.

Acknowledgments

The authors are grateful for the financial supports from the National Natural Science Foundation of China (51971205), Shenzhen Science and Technology Innovation Program, China (JCYJ20190807154005593), and the Fundamental Research Funds for the Central Universities, China (19lgpy20).

References

[1] LORIA E A. Gamma titanium aluminides as prospective structural materials [J]. Intermetallics, 2000, 8(9): 1339−1345.

[2] APPEL F, CLEMENS H, FISCHER F. Modeling concepts for intermetallic titanium aluminides [J]. Progress in Materials Science, 2016, 81: 55−124.

[3] CHEN Guang, PENG Yin-bo, ZHENG Gong, QI Zhi-xiang, WANG Min-zhi, YU Hui-chen, DONG Cheng-li, LIU C T. Polysynthetic twinned TiAl single crystals for high-temperature applications [J]. Nature Materials, 2016, 15: 876.

[4] LIN Jun-pin, ZHAO Li, LI Gang-yang, ZHANG Lai-qi, SONG Xi-ping, YE Feng, CHEN G L. Effect of Nb on oxidation behavior of high Nb containing TiAl alloys [J]. Intermetallics, 2011, 19(2): 131−136.

[5] GONG Xue, CHEN Rui, FANG Hong-ze, DING Hong-sheng, GUO Jing-jie, SU Yan-qing, FU Heng-zhi. Synergistic effect of B and Y on the isothermal oxidation behavior of TiAl−Nb−Cr−V alloy [J]. Corrosion Science, 2018, 131: 376−385.

[6] GARIP Y, OZDEMIR O. Comparative study of the oxidation and hot corrosion behaviors of TiAl−Cr intermetallic alloy produced by electric current activated sintering [J]. Journal of Alloys and Compounds, 2019, 780: 364−377.

[7] ZHANG Kai, LI Zheng-wei, GAO Wei. Hot corrosion behaviour of Ti−Al based intermetallics [J]. Materials Letters, 2002, 57(4): 834−843.

[8] ELIAZ N, SHEMESH G, LATANISION R M. Hot corrosion in gas turbine components [J]. Engineering Failure Analysis, 2002, 9(1): 31−43.

[9] GODLEWSKA E, MITORAJ M, LESZCZYNSKA K. Hot corrosion of Ti−46Al−8Ta (at.%) intermetallic alloy [J]. Corrosion Science, 2014, 78: 63−70.

[10] RUBACHA K, GODLEWSKA E, MARS K. Behaviour of a silicon-rich coating on Ti−46Al−8Ta (at.%) in hot-corrosion environments [J]. Corrosion Science, 2017, 118: 158−167.

[11] RAPP R A, GOTO K. The hot corrosion of metals by molten salts [J]. ECS Proceedings Volumes, 1981, 1981: 159−177.

[12] STEINMETZ P, DURET C, MORBIOLI R. Laboratory tests for hot-corrosion studies [J]. Materials Science and Technology (United Kingdom), 1986, 2(3): 262−271.

[13] RAPP R A. Hot corrosion of materials: A fluxing mechanism? [J]. Corrosion Science, 2002, 44(2): 209−221.

[14] NICHOLLS J R, LEGGETT J, ANDREWS P. Hot salt corrosion of titanium aluminides [J]. Materials and Corrosion, 1997, 48(1): 56−64.

[15] YAO Z, MARCK M. NaCl-induced hot corrosion of a titanium aluminide alloy [J]. Materials Science and Engineering A, 1995, 192−193: 994−1000.

[16] JIN Guang-xi, QIAO Li-jie, GAO Ke-wei, KIMURA T, HASHIMOTO K. Effect of Mn and V on hot corrosion of TiAl alloy [J]. Acta Metallurgica Sinica, 2004, 40(3): 179−184.

[17] CISZAK C, POPA I, BROSSARD J M, MONCEAU D, CHEVALIER S. NaCl induced corrosion of Ti−6Al−4V alloy at high temperature [J]. Corrosion Science, 2016, 110: 91−104.

[18] WU Xin-hua. Review of alloy and process development of TiAl alloys [J]. Intermetallics, 2006, 14(10): 1114−1122.

[19] MITORAJ-KRÓLIKOWSKA M, GODLEWSKA E. Hot corrosion behaviour of (γ+α_2)−Ti−46Al−8Nb (at.%) and α-Ti−6Al−1Mn (at.%) alloys [J]. Corrosion Science, 2017, 115: 18−29.

[20] TANG Zhao-lin, WANG Fu-hui, WU Wei-tao. Effect of a sputtered TiAlCr coating on hot corrosion resistance of gamma-TiAl [J]. Intermetallics, 1999, 7(11): 1271−1274.

[21] TANG Zhao-lin, WANG Fu-hui, WU Wei-tao. Effect of Al_2O_3 and enamel coatings on 900 °C oxidation and hot corrosion behaviors of gamma-TiAl [J]. Materials Science and Engineering A, 2000, 276(1): 70−75.

[22] LI Wei-bo, LIU Lan-lan, YANG Ying-fei, ZHU Sheng-long, WANG Fu-hui. Hot corrosion behavior of SiO_2−Al_2O_3−glass composite coating on Ti–47Al–2Cr–2Nb alloy:

Diffusion barrier for S and Cl [J]. Acta Metallurgica Sinica (English Letters), 2019, 32(5): 599−606.

[23] LIN Hao, LIANG Wen-ping, JIA Yan-lin, MIAO Qiang, HU Rong-yao, DING Zheng, YU Li-jia. Effect of AlY gradient coating on hot corrosion resistance of γ-TiAl alloy at different temperatures [J]. Applied Surface Science, 2019, 487: 868−875.

[24] ZHANG Kun, ZHANG Tie-bang, ZHANG Xu-hu, SONG Lin. Corrosion resistance and interfacial morphologies of a high Nb-containing TiAl alloy with and without thermal barrier coatings in molten salts [J]. Corrosion Science, 2019, 156: 139−146.

[25] MI Feng-yi, ZHU Sheng-long. Long-term high temperature oxidation and hot corrosion behavior of an enamel coating on γ-TiAl intermetallics at 700 °C [J]. Corrosion Science and Protection Technology, 2015, 27(3): 254−258.

[26] BACOS M P, THOMAS M, RAVIART J L, MOREL A, MERCIER S, JOSSO P. Influence of an oxidation protective coating upon hot corrosion and mechanical behaviour of Ti−48Al−2Cr−2Nb alloy [J]. Intermetallics, 2011, 19(8): 1120−1129.

[27] TIAN Zong-jun, GAO Xue-song, HUANG Yin-hui, LIU Zhi-dong, SHEN Li-da, WANG Dong-sheng. Study on hot corrosion behavior of plasma-sprayed NiCoCrAl−Y_2O_3 coating on TiAl alloy surface [J]. Rare Metal Materials and Engineering, 2010, 39(8): 1439−1442. (in Chinese)

[28] WANG Dong-sheng, TIAN Zong-jun, SHEN Li-da, HUANG Yin-hui. Hot corrosion resistance of plasma-sprayed MCrAlY coatings by laser remelting on TiAl alloy surface [J]. Transactions of the China Welding Institution, 2014, 35(8): 17−20.

[29] LI Shan, LIANG Wen-ping, MIAO Qiang, DING Zheng, WANG Xu. Hot corrosion behavior of Al−Y gradient coating on γ-TiAl alloy in sulfate at 850 °C [J]. Heat Treatment, 2018, 33(1−6).

[30] MO Min-hua, WU Lian-kui, CAO Hua-zhen, LIN Jun-pin, ZHENG Guo-qu. Improvement of the high temperature oxidation resistance of Ti−50Al at 1000 °C by anodizing in ethylene glycol/BmimPF_6 solution [J]. Surface and Coatings Technology, 2016, 286: 215−222.

[31] MO Min-hua, WU Lian-kui, CAO Hua-zhen, LIN Jun-pin, LU Dong-hui ZHENG Guo-qu. High temperature oxidation behavior and anti-oxidation mechanism of Ti−50Al anodized in ionic liquid [J]. Surface and Coatings Technology, 2016, 307: 190−199.

[32] MO Min-hua, WU Lian-kui, CAO Hua-zhen, LIN Jun-pin, ZHENG Guo-qu. Halogen effect for improving high temperature oxidation resistance of Ti−50Al by anodization [J]. Applied Surface Science, 2017, 407: 246−254.

[33] WU Lian-kui, XIA Jun-jie, CAO Hua-zhen, LIU Wen-juan, HOU Guang-ya, TANG Yi-ping, ZHENG Guo-qu. Improving the high-temperature oxidation resistance of TiAl alloy by anodizing in methanol/NaF solution [J]. Oxidation of Metals, 2018, 90(5−6): 617−631.

[34] WU Lian-kui, XIA Jun-jie, JIANG Mei-yan, WANG Qi, WU Hai-xin, SUN Dong-bai, YU Hong-ying, CAO Fa-he. Oxidation behavior of Ti45Al8.5Nb alloy anodized in NH_4F containing solution [J]. Corrosion Science, 2020: 108447.

[35] WANG Hong-yu, ZHANG Xiang, XU Zeng, WANG Han, ZHU Chang-shun. Hot corrosion behaviour of Al−Si coating in mixed sulphate at 1150 °C [J]. Corrosion Science, 2019, 147: 313−320.

[36] NICHOLLS J R. Designing oxidation-resistant coatings [J]. The Journal of The Minerals, Metals & Materials Society, 2000, 52(1): 28−35.

[37] WU Lian-kui, WU Jin-jia, WU Wei-yao, HOU Guang-ya, CAO Hua-zhen, TANG Yi-ping, ZHANG Hui-bin, ZHENG Guo-qu. High temperature oxidation resistance of γ-TiAl alloy with pack aluminizing and electrodeposited SiO_2 composite coating [J]. Corrosion Science, 2019, 146: 18−27.

[38] XIANG Zhi-dong, ROSE S, DATTA P K. Pack deposition of coherent aluminide coatings on γ-TiAl for enhancing its high temperature oxidation resistance [J]. Surface and Coatings Technology, 2002, 161(2): 286−292.

[39] JUNG H G, KIM K Y. Effect of ternary elements on the oxidation behavior of aluminized TiAl alloys [J]. Oxidation of Metals, 2002, 58(1): 197−216.

[40] GAUTHIER V, DETTENWANGER F, SCHÜTZE M, SHEMET V, QUADAKKERS W. Oxidation-resistant aluminide coatings on γ-TiAl [J]. Oxidation of Metals, 2003, 59(3−4): 233−255.

[41] CHEN Lin-cong, ZHANG Chi, YANG Zhi-gang. Effect of pre-oxidation on the hot corrosion of CoNiCrAlYRe alloy [J]. Corrosion Science, 2011, 53(1): 374−380.

[42] SCHÜTZE M. The role of surface protection for high-temperature performance of TiAl alloys [J]. The Journal of The Minerals, Metals & Materials Society, 2017, 69(12): 2602−2609.

[43] TSIPAS S A, GORDO E, JIMÉNEZ-MORALES A. Oxidation and corrosion protection by halide treatment of powder metallurgy Ti and Ti6Al4V alloy [J]. Corrosion Science, 2014, 88: 263−274.

[44] SCHUMACHER G, LANG C, SCHÜTZE M, HORNAUER U, RICHTER E, WIESER E. Improvement of the oxidation resistance of gamma titanium aluminides by microalloying with chlorine using ion implantation [J]. Materials and Corrosion, 1999, 50(3): 162−165.

[45] XU Yi, LIANG Wen-ping, MIAO Qiang, WANG Ling, REN Bei-lei, CUI Shi-yu, XIA Jin-jiao, YAO Zheng-jun. Enhanced high temperature corrosion resistance of Al_2O_3/Al composite coating on gamma-TiAl alloy [J]. Rare Metal Materials and Engineering, 2018, 47(4): 1075−1081.

阳极氧化和预氧化提高渗铝 TiAl 合金的热腐蚀性能

胡远涛[1,2]，郑 磊[3]，严豪杰[1,2]，伍廉奎[1,2]，林向军[3]，曹发和[1]，蒋梅燕[2]

1. 中山大学 材料科学与工程学院，广州 510275；
2. 浙江工业大学 材料科学与工程学院，杭州 310014
3. 中国人民解放军军事科学院 国防工程研究院，北京 100850

摘 要：为提高 TiAl 合金的抗热腐蚀性能，采用渗铝、阳极氧化和预氧化技术在 TiAl 合金表面制备致密的防护涂层。研究 700 °C 下涂层保护的 TiAl 合金在 75% Na_2SO_4 + 25% NaCl(质量分数)熔盐环境中的热腐蚀行为。结果表明，阳极氧化和预氧化可促进 Al_2O_3 防护层的形成，有效阻止热腐蚀环境下熔融盐和氧气向基体的扩散。在热腐蚀过程中，渗铝层为致密 Al_2O_3 层的持续形成提供铝元素。另外，预氧化后渗铝层中形成由 $TiAl_3$ 和 $TiAl_2$ 组成的梯度扩散层，降低涂层内部的应力。

关键词：热腐蚀；TiAl 合金；包埋法；阳极氧化；卤素效应

(Edited by Xiang-qun LI)